Earth Atmosphere Observatory Formation at L2

Edward Mettler,* A. Behçet Açıkmeşe, William G. Breckenridge,
Steven A. Macenka , Eldred F. Tubbs

Jet Propulsion Laboratory, California Institute of Technology,
4800 Oak Grove Dr., Pasadena, CA 91109-8099

This paper is a product of research supported by NASA under RASC (the Revolutionary Aerospace Systems Concepts) program. It presents an overall system architecture, and covers issues of deployment, navigation, and control related to a formation of two spacecraft in the neighborhood of the Sun-Earth L2 Lagrange point (on the Sun-Earth line), that serves as an observatory of Earth's atmosphere.

The observatory concept definition study was a multi-center NASA effort conducted in 2003, and covered a much wider scope than is presented in this focused paper.

The Earth observatory at L2 is a unique design concept that can improve the knowledge and understanding of dynamic, chemical and radiative mechanisms that cause changes in the atmosphere, and can lead to the development of models and techniques to predict short and long-term climate changes.

I. Introduction

In this paper, we describe the overall system architecture of a revolutionary Earth Atmosphere Observatory Formation concept, and discuss the deployment, guidance, navigation, and precision control methods for the formation of two spacecraft in orbit in the neighborhood of the Sun-Earth L2 (Lagrange) point, and station-keeping on the Sun-Earth line at approximately 1.5 million kilometers from the Earth, to observe the Earth in continuous occultation of the sun. This formation is composed of a Secondary Telescope spacecraft, pointed at a 25-meter membrane mirror on a Primary Aperture spacecraft 125-meters distant on-axis in formation flying precision alignment, that scans the focused image of the illuminated atmosphere of the Earth reflected from the large mirror. We developed a unique optical system design to meet the specific science requirements of high resolution (within one km of atmosphere height) over a spectral wavelength range of 0.28 microns to 10.5 microns. Figures 1 and 2 depict this concept's unique design that can provide a revolutionary advance in the knowledge and understanding of the dynamic mechanisms that cause changes in the atmosphere, leading to the development of models and techniques for prediction of short and long-term climate changes.

The Sun-Earth L2 is an actual equilibrium point of the two body problem described by Sun and Earth. The only other significant gravitational force is due to the Moon so that an actual equilibrium point is not at Sun-Earth L2, but it is at the very close proximity of the Sun-Earth-Moon Barycenter L2 point. Our objective is for the observatory to track a point on the Sun-Earth line in the neighborhood of the Sun-Earth L2 point, with a minimum penalty of fuel use.

There are strong scientific motivations for placing an Earth observatory at L2 [a] Occultation is best suited for long-term climate change studies from L2, and L2 is the optimal place to deploy solar occultation instruments. We can obtain high vertical and spatial resolution maps of many species twice per day for use in near-real time predictive assimilation models. Improvements over current practice will be dramatic with 10 times improvement over EOS Aura through a combination of increased instrument sampling and algorithmic techniques. Trend-Quality observations of the dynamical response of the middle atmosphere (10-70km) to climate change will be possible. A similar capability would require a constellation of multiple spacecraft in low Earth orbit. Near real-time production of final products for time-critical consumption (forecast models) will be feasible. The observatory will be able to remain close to the Earth-Sun axis for a 24/7 100% duty cycle. It will scan around the annular ring of the Earths atmosphere at least 360 times per day for 1° longitudinal sampling. It will sample each rotation of the Earth at least 360 times to provide 1° latitudinal sampling. Refraction will limit the lowest altitude to approximately 8km. Co-alignment of all instruments and synchronized operations will provide sampling of the same air mass over all wavelengths (0.25 to 10.5 microns). Other measurement metrics include a Vertical Resolution of 1 km, Vertical Range of 8 to 100 km, Altitude Knowledge of 100 m, Global Mapping Twice per day, Continuous Mapping is provided, and the number of Profiles per day is 160 thousand to 2 million.

---

*Senior Member AIAA, Observatory PI and Architect.

[a]We wish to gratefully acknowledge Dr. J. Zawodny of NASA LaRC for his role as scientific PI for this study.

Strategies for atmospheric monitoring will involve global maps of the vertical distribution of O_3, CO_2, CH_4, H_2O, N_2O, key members of the NO_x and CL_x, and upper tropospheric and stratospheric clouds, sulfate aerosol mass, temperature, and pressure with sampling near the stratopause, twice per day. Long-lived species will be used to monitor the global circulation (mean meridional and planetary wave dynamics) at a lower vertical resolution , and observations will be made of changes in the tropopause region and stratospheric-tropospheric exchange processes.

These capabilities will enable the L2 Observatory to determine changes in the forcing and response of the Earths atmosphere; to understand the mechanisms of change and quantify the attribution of change, be it of chemical or dynamical origin; to improve the short and long term predictive capability of weather and climate models through the use of near real time measurements and an improved understanding of the dynamical, chemical, and radiative feedbacks and responses of the climate system.

Our observatory concept definition identifies the key technology advances required of current electric propulsion technology, as well as for optical metrology sensors, and ultra-lightweight actively controlled membrane mirror technology that will enable this mission. With these feasible developments over the current and following decade, we will be able to realize the benefits of an Earth Atmosphere Observatory at L2.

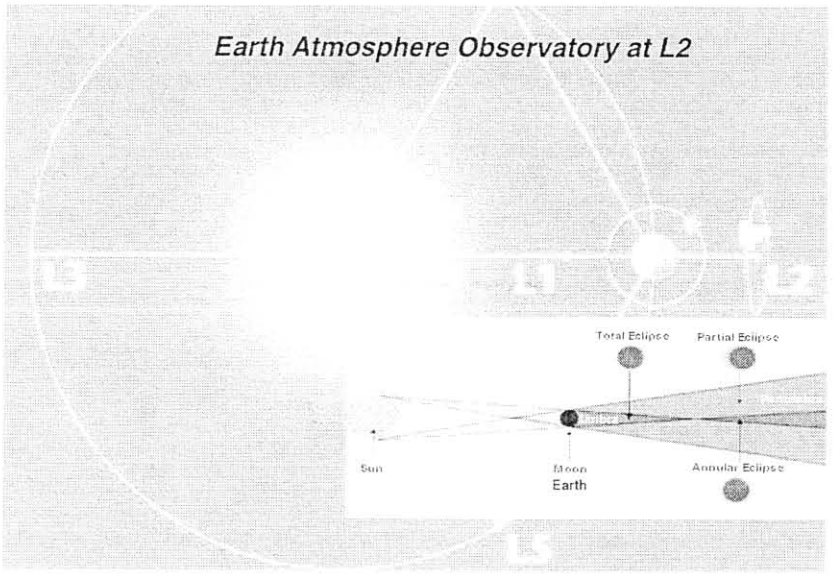

Figure 1. L2 Observatory Concept

II. System Architecture

The proposed observatory at L2 is a formation of two spacecraft, Figure 3, *science* (S/C-S) and *large aperture* (S/C-A) spacecraft. S/C-S is located between S/C-A and Earth, and it is equipped with a science telescope pointing at a large mirror on S/C-A, attached to a bus (see figures 4, 5). The bus module of both spacecraft has the engineering equipment: sensors, reaction wheels, thrusters, communication equipment etc. The image reflected by the membrane mirror is scanned by this telescope (figures 5, 6) that has a corrector mirror to correct for the spherical abberations caused by the membrane mirror.

S/C-A is 125 meters away from S/C-S on Sun-Earth line. It has an $f/5$ spherical membrane mirror, with a 25 meter outer and 7 meter inner diameter that is supported by inflatable torus in the outer and inner diameters. There is an engineering bus at the center of the large mirror that contains guidance and control hardware. The Primary Aperture is 25 m diameter to satisfy science 1 km resolution at Earth over broadband spectrum, i.e. diffraction limit of 67 micro-radian at 10.5 microns. Then, the theoretical size requirement for this large aperture is 19 m with added margin for membrane boundary conditions. The Earth-Sun are extended objects viewed from L2, and they require a **Spherical Aperture** system or **Schmidt Telescope** concept to handle *wide angle and high resolution*.

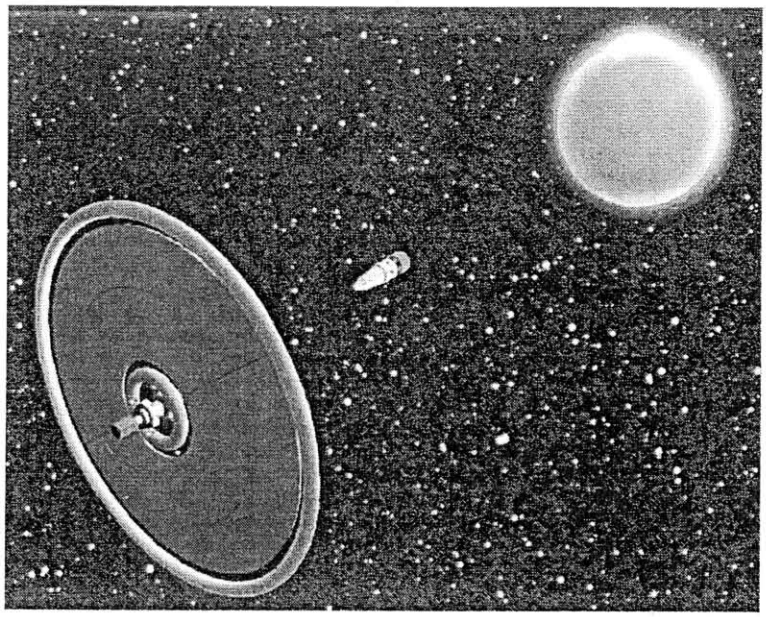

Figure 2. Earth Atmosphere Observatory Formation at L2 Viewing Solar Occultation by Earth

First a spherical mirror with a focal ratio of $f/10$ was considered. This implies a focal length of 250 m, and a center of curvature of 500 m. The Schmidt spherical aberration **Corrector Mirror**, normally located at the center of curvature in a monolithic system, must be re-imaged to locate inside the Science S/C Telescope (figures 6, 7, 8). This is called a *Reduced Schmidt* design and adds complexity. However, the desired f/10 optics creates an excessively large (2.5 m) Solar Light Annulus image at the Primary focal plane. So, the optical system design is constrained to a practical $f/5$ with annulus size of 1.25 m, in order to keep the Science Telescope optics and S/C size/mass within realistic limits. The $f/5$ (see Figure 6) telescope assembly mass is less than 10% of the mass of the $f/10$ telescope. However, this significant reduction in mass comes with some other design challenges, and some of those are:

- Faster $f/5$ primary mirror is more prone to spherical aberration and less depth of field tolerance.
- Smaller size relay and corrector elements required for $f/5$ mirror are more difficult to design (Lagrange invariant) for required performance.
- Ratio of 25 m to 1 m pupil magnification increases distortion.
- Greater number of optical elements required reduces broadband energy throughput of optical train.
- Required Corrector Aspheric is more complex to design and fabricate.
- A *fast steering mirror* is required for beam stabilization.

III. System Requirements

The main science requirements are:

- Earth atmospheric observation from the neighborhood of Earth-Sun point.
- Scan the Earth atmosphere within 100 km of the surface (latitude, longitude $\pm 90°$).
- Sample the atmosphere with 1 km vertical resolution in increments of 1 degree latitude and longitude.
- Navigate in 200k km radius tube around Sun-Earth line to maintain Sun annulus around Earth.
- Large aperture telescope for a resolution of less than 0.67 μrad for observations at wavelengths 0.28 μm to 10.5 μm.
- Angular jitter less than 0.13 arc-sec (0.63 μrad) (peak-peak) for frequencies larger than 100 Hz.
- Knowledge of control jitter to less than 0.2 km for lower frequencies.

The science requirements above impose specific engineering requirements on the system. Some of these requirements, and the error allocations are summarized below:

Requirements on navigation, and error allocation:

- Lateral position from the Sun-Earth line $\leq 200km$.
  - Sun-Earth line offset knowledge $\rightarrow$ 100 km (3-σ value: 63 km for unfiltered Earth centroid knowledge, 63 km for unfiltered Sun centroid knowledge.
  - Formation position control $\rightarrow$ 100 km.
- Allowable Earth range variation $\rightarrow \pm$ 5000 km.
- Earth relative pointing: Communication using HGA $\rightarrow \pm$ 436 μrad.
  - Earth direction, Earth-Sun sensor centroid, 3-σ unfiltered $\rightarrow$ 42 μrad.
  - Pointing control $\rightarrow \pm$ 175 μrad.
  - HGA misalignment with respect to Earth-Sun sensor, 3-σ, $\rightarrow$ 80 μrad.

Requirements on formation, and error allocation:

- Image position error perpendicular to LOS (line of sight) in order to fit within a 5 cm telescope entrance aperture $\rightarrow \pm 2$ cm.
  - Mirror knowledge, optical metrology (3-σ filtered) $\rightarrow$ 0.21 cm.
  - Earth direction, Earth-Sun sensor centroid (3-σ filtered) $\rightarrow$ 0.53 cm.
  - 5m aperture offset times S/C pointing control error $\rightarrow$ 0.03 cm.
  - Relative position control error $\rightarrow \pm$ 1 cm.

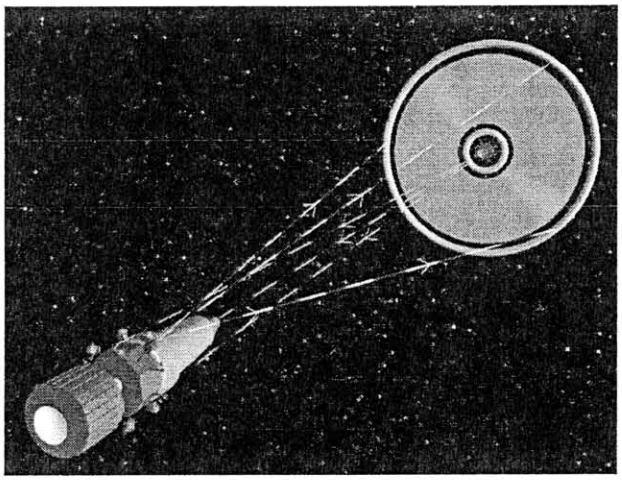

Figure 3. Observatory Formation Performing Relative Range and Bearing Alignment with Autonomous RF Metrology (We gratefully acknowledge S. Krizan of NASA LaRC for his observatory CAD support for Telescope CAD design)

IV. Sensors

The following sensors are used in this mission:

1. **Formation RF metrology**: It provides GPS-like range and phase measurements between transmitter and receiver, which are triangulated to get relative position and attitude of S/C-A for acquisition and coarse formation

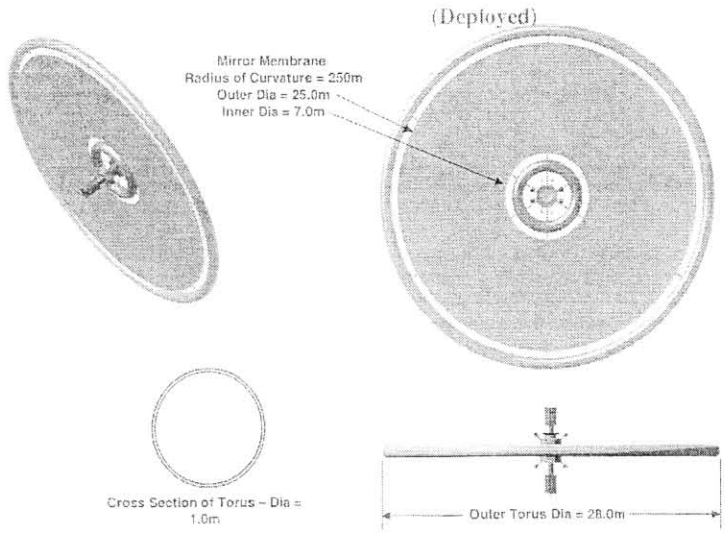

Figure 4. Large Aperture Spacecraft

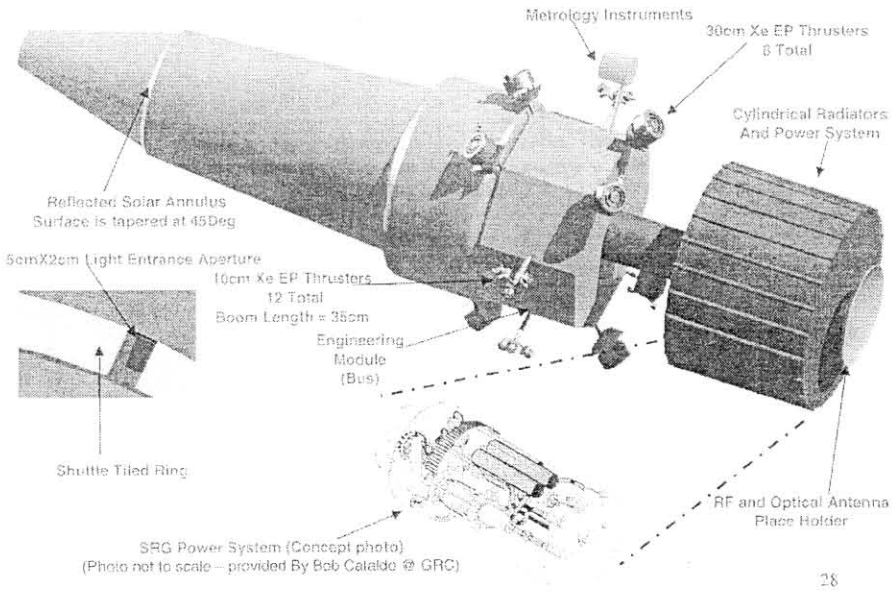

Figure 5. Science Spacecraft (We gratefully acknowledge R. Hein for Telescope CAD design)

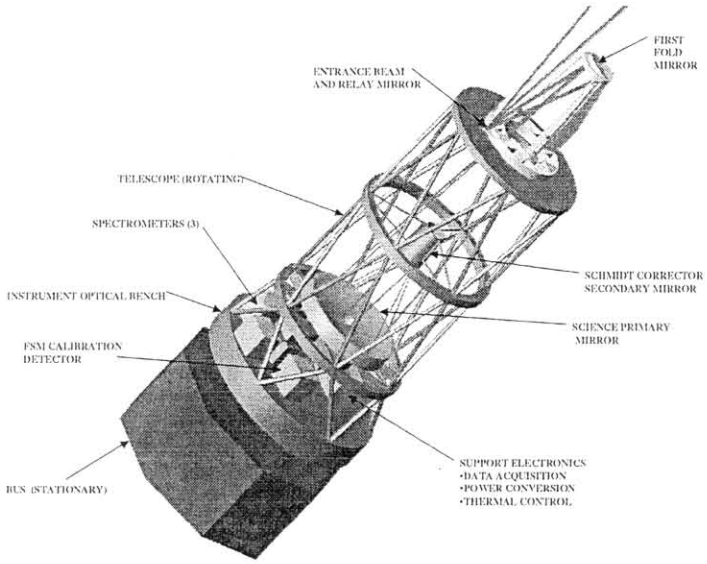

Figure 6. Science Telescope

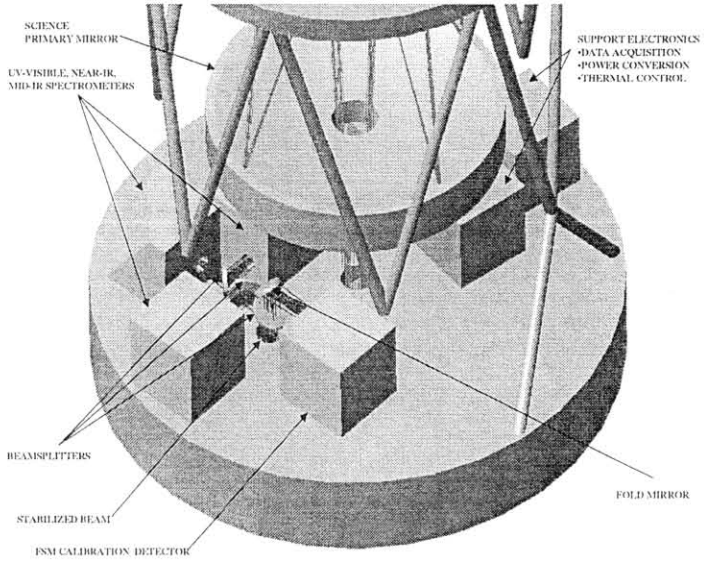

Figure 7. Science Telescope

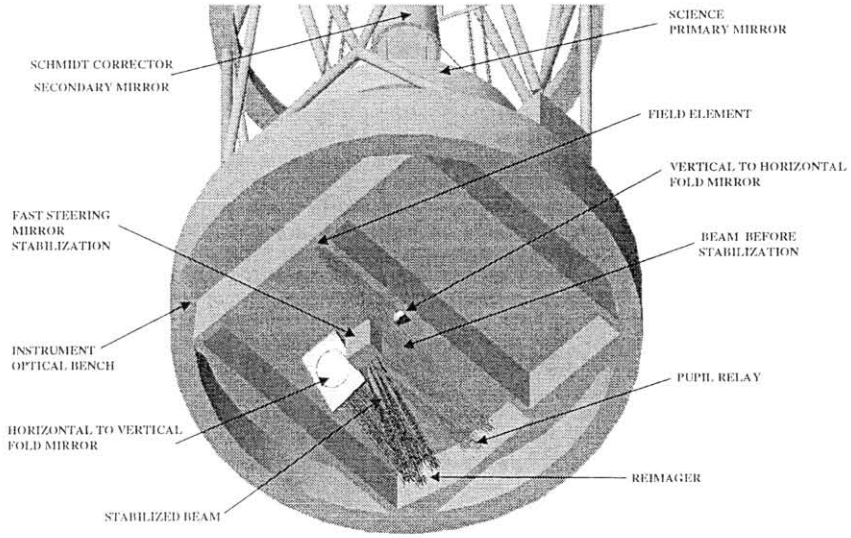

Figure 8. Science Telescope

control (Figure 9). This metrology suite will use JPL's existing "TurboRogue" transceivers, which are readily adaptable to variable baselines from 100m to a 1 km separation. The current capability for measurement precision ($1-\sigma$ values) are: (i) 1 cm relative range, (ii) 1 arc-min relative orientation, and (iii) 0.1 mm/s relative velocity.

2. **Earth-Sun sensor**: This sensor images Earth and Sun to find points on the limbs, and determine: relative Earth direction, position offset from Sun-Earth line, and course Earth range (Figure 10).
3. **Optical Metrology**: The optical metrology performs two functions by operating in two different modes. In the first mode, optical metrology uses a laser that is reflected back from several (3-4) retro-reflectors placed on outer and inner toroidal circumferences of the mirror, and one in the center of the mirror, to precisely measure relative formation range and bearing, attitude, and zeroth order mirror shape (tip, tilt, and piston) for fine formation control and Earth image location prediction. The current capability for measurement precision are: (i) 1 micro-m relative range, and (ii) 10 micro-rad relative bearing. The second mode of the optical metrology is the operation as a mirror surface figure sensor.
4. **Surface-figure sensor**: The Surface-Figure Sensor uses a new interferometric technology: Modulation Sideband Technology for Absolute Ranging (MSTAR) together with precision angular measurement to determine the three-dimensional location of retro-reflective targets on the surface of the primary mirror (Figure 11). The MSTAR system is described by Lay et al.[1]
5. **Center-of-curvature sensor**: The center-of-curvature sensor provides initial test of the quality of the spherical shape of the mirror (Figure 12).
6. Standard spacecraft sensor suite, inertial measurement units: sun sensor, and star trackers.

The sensors 1-5 in this list are mission specific sensors, where as item 6 describes the standard guidance and control sensors.

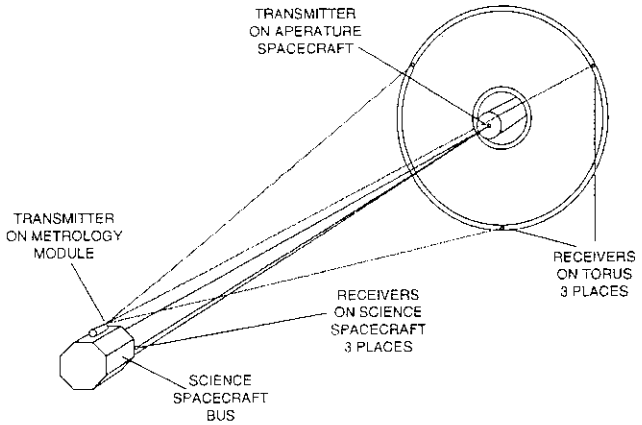

Figure 9. RF Metrology

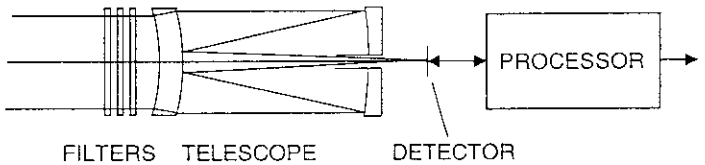

Figure 10. Earth-Sun Sensor

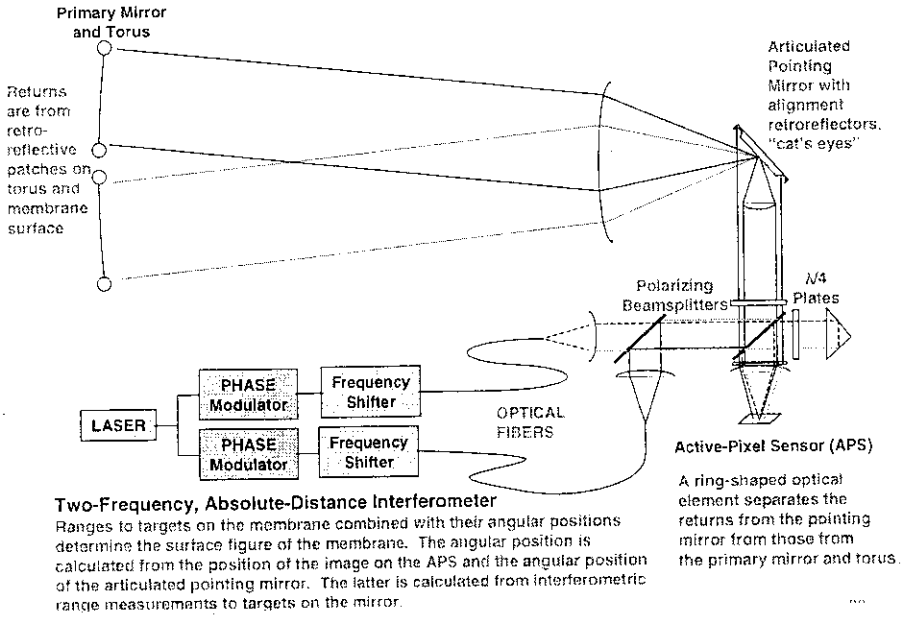

Figure 11. Optical Metrology and Figure Sensor

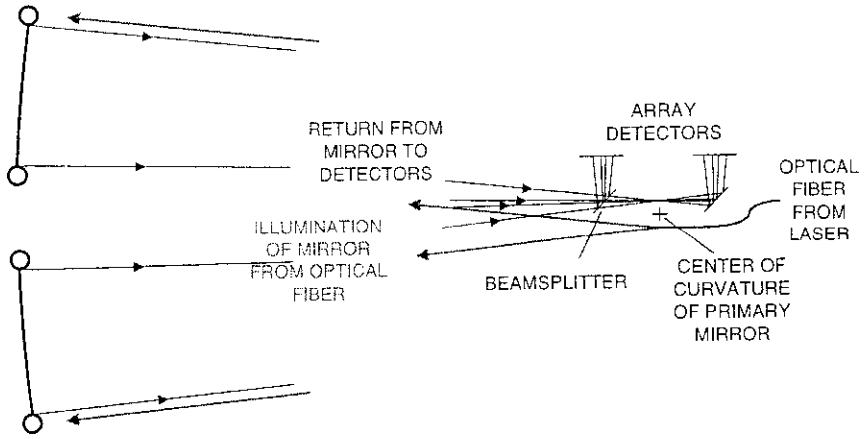

Figure 12. Center-of-curvature Sensor

V. Delivery

Both spacecraft are delivered to Sun-Barycenter L2 (here Barycenter refers to the center of mass of Earth and Moon) by a single carrier spacecraft, which must move away a safe distance before returning home (see[2] for delivery mission design and navigation analysis). Our later orbital analysis suggests an orbit for the observatory that follows a point on Sun-Earth line that is the projection of the Sun-Barycenter L2 point on the Sun-Earth line. Therefore, this orbit point on Sun-Earth line coincides with the Sun-Barycenter L2 point twice a month, providing frequent rendezvous opportunities.

Simple geometrical computations (by using Earth's mean distance from Sun, Earth and Sun radius, mean distance of Sun-Barycenter L2 point from Earth), show that the delivery accuracy to the Sun-Barycenter L2 point should be less than 7000 km in normal direction, in order to have at least half of the Sun occulted for operation of the Sun-Earth sensor. And, there is no occultation beyond 13000 km in normal direction. This requirement can be relaxed an additional 5000 km for the tangential direction, because of larger space that Sun-Earth line sweeps in this direction. In that case, we just have to wait until the occultation is at a desirable level.

A. Deployment from Carrier

First major step in in deployment is the separation of the spacecraft from the carrier. Each spacecraft must be turned on, necessary checks must be performed for autonomous operations prior to the separation. Position and attitude estimators should also be initialized and operational. The carrier is responsible for controlling the separation direction, so that separation path of both spacecraft shall not intersect (to avoid possible collision if a spacecraft is uncontrolled).

After the separation, each spacecraft will:

- Assume a specified attitude.
- Stop after moving a specified distance (specified stopping points should allow RF acquisition).
- Deploy stowed appendages.
- Establish inter-spacecraft communication (ISC) and RF metrology as soon as possible.

After separation, relative position is propagated in an open-loop mode. The separation distance of the stopping points should be consistent with the expected accuracy to avoid collision. Also, acquiring RF metrology is necessary to improve the relative position knowledge accuracy , and further prevent the possibility of collision due to growing open loop estimation errors. The RF metrology accuracy will be significantly improved once the primary mirror is deployed, but it should be adequate for collision avoidance until then.

At this point, one of the spacecraft can be designated as a *leader* and the other as the *follower* for mission executive control purposes. We do not use a leader follower structure in our formation flying control algorithm. In this regard, orbit following, and formation relative position control are independently designed, and they can also be decoupled in terms of actuation (since we use small and large thrusters that can be dedicated to formation and orbit control).

Until this point in deployment, the absolute position knowledge is only available from ground tracking and orbit determination.

B. Sun-Earth Acquisition

When the delivery requirement is met, the spacecraft should see the Earth occulting the Sun image at this stage. The degree and form of the occultation depends on the accuracy of the delivery and time of the month (note that even if the delivery is with perfect accuracy, since Sun-Barycenter L2 point is only on Sun-Earth line twice a month, we see different degrees of occultation from this point). The information on inertial Sun-Barycenter vector, the offset vector of Earth from Earth-Moon barycenter are obtained from ephemeris data. The Earth-Sun sensor is then used to estimate the center of Earth shadow and Sun limb images (for which the accuracy will be reduced if there is a partial limb). For the absolute delivery accuracy with respect to the Sun-Barycenter line, the Sun direction can be mapped to inertial coordinates by using the attitude information. Unless this error is so large that it affects the expected occultation, it does not need to be corrected. Also, note that we can estimate the velocity over time.

Then, the rendezvous with Sun-Earth line is to be planned based on data from the estimation of Sun-Earth line offset, and its rate of change. This offset is roughly ± 5000 km over a monthly cycle, and the degree of occultation also varies, with the most accurate measurements obtained when there is a complete Earth shadow. Here, we can also estimate the Earth's diameter, thus the range from Earth. However, it will require intensive filtering to obtain an estimate accurate enough to use for rendezvous in the radial direction.

In a uniformly rotating coordinate frame with the origin at Sun-Barycenter L2, the ephemeris data provides the motion (position and velocity) of the orbit point on Sun-Earth line. The Sun-Earth offset estimate from Earth-Sun sensor is used to estimate the position and velocity of the spacecraft in this coordinate system. Using these information, a propulsive rendezvous maneuver should be designed to move from spacecraft state (position/velocity) to a future target point (orbit point) state. After, the rendezvous is successfully completed, the spacecraft will follow the orbit point acceleration profile. This maneuver is designed by solving an optimization problem, where fuel or maneuver time is minimized with acceleration constraints. and is the subject of future development.

C. Absolute/Relative Positioning

Once the orbit point rendezvous is accomplished, the spacecraft follow the orbit point acceleration profile by using feed-forward actuation, and feedback actuation for necessary orbit corrections via the information provided by Earth-Sun sensor. The tracking accuracy of the orbit must be in specified limits. The formation accuracy is not fine enough yet, but it is to a level of accuracy that is sufficient in terms of avoiding collisions and area of focused sunlight.

At this stage of deployment, we should already have the primary mirror deployed. If it is not yet deployed, it must be done now, before proceeding further in this sequence of events. Once the ground verifies deployment, we can proceed to the next step. Note that, the monitoring of the deployment for ground verification would be by some imaging sensor, which has not yet been defined.

After a stable configuration is achieved, the Science spacecraft is moved to the center of curvature (250 m away from the Primary mirror), which is at a sufficient distance from focused sunlight.

The fine positioning of the Science spacecraft is achieved by using first the formation RF sensor, then using the optical-metrology sensor. This adjustment is done until, we can activate the Center-of-Curvature sensor, which is used to provide the final positioning of the Science spacecraft. Center-of-curvature sensor will also determine the quality of the spherical shape of the mirror.

At this point, optical metrology surveys the surface of the mirror, and the mirror shape is estimated. Then, the mirror shape control is initiated and applied until the shape is is within the required tolerance. Once the mirror shape is adjusted, the position of the Sun-Earth image from the Primary mirror is determined in large aperture spacecraft coordinates by using the attitude information and inertial direction to the Earth.

Now, the telescope in the Science spacecraft must be rotating to sample the image, which was not required before. Then, the Science spacecraft is moved in order to place the center of rotation of the entrance aperture at the predicted center of the Sun-Earth image. The relative position is measured using the RF and optical metrology for the closed loop formation flying control. At this point, the telescope entrance aperture should be scanning the Earth limb.

The *limb detector* in the science telescope then determines the true limb position, and controls the fast steering mirror to place the limb in the Science Sensor field of view. The same correction can be applied as a vernier control on the Science spacecraft position relative to the image, correcting for errors in the image location prediction, and relative position control. This completes the deployment, and the formation is ready to collect science data.

VI. Different Orbits Under Consideration

The first orbit under consideration is a point on Sun-Earth line which is 1.51 million km away from Earth. This is Sun-Earth L2 point[3] if the trajectory of Earth around Sun is assumed to be a perfect circle. Then, we consider the Sun-Earth L2 point with the actual orbit of Earth around Sun obtained either from a three body simulation of Sun-Earth-Moon, or from prescribed orbits of Sun-Earth-Moon. A third orbit is also considered, which has the least severe ΔV requirement among the three. This orbit is constructed by projecting Sun-Barycenter L2 onto the Sun-Earth line. The computation of Sun-Barycenter L2 point is done by lumping Earth-Moon mass onto Barycenter, which is located at the mass center of Sun and Moon. The reduction in ΔV requirements are observed to be significant (nearly half of the former ones), and this cylindrically constrained orbit also satisfies all science requirements. Therefore, we will refer to this orbit as the "optimal orbit on Sun-Earth line" for all practical purposes.

We name these orbits as Orbit-1,2, and 3 in the order mentioned above, i.e. Orbit-1 is the orbit with fixed distance from Earth, Orbit-2 is point at Sun-Earth L2 point, and Orbit-3 is the point at the projection of Sun-Barycenter L2 point on Sun-Earth line [b].

[b]We would like to gratefully acknowledge Carlos Roithmayr, Spacecraft and Sensors Branch, NASA LaRC for his important observation of cylindrical constraint boundary to the orbit motions of the observatory.

ΔV is computed by using 1 and 2-norm of the inertial acceleration vector of the orbit point, i.e.

$$\Delta V_{avg_{1,2}} = \frac{1}{N} \int_0^T \|\vec{a}_N(t)\|_{1,2} \, dt \, , \tag{1}$$

where, $\vec{a}_N$ is the net inertial acceleration, and N is the number of days in time period T. Then, we also computed ΔV requirements in radial, tangential, and normal directions. Radial direction is the direction from Earth to the point (which is same as the direction described by Sun-Earth line), and tangential and normal directions describe the plane normal to the radial direction. It is assumed that Earth-Moon orbit and Sun-Barycenter orbit are independent from each other, and they are solved by using two body formulations. The Sun-Barycenter and Earth-Moon orbits have prescribed eccentricities. Also, the Earth-Moon orbit around the Barycenter is assumed to have 5.15 degrees of inclination with respect to the plane described by the orbit of Barycenter around Sun. The numerical computations are performed for a time period of a year. The results are:

Orbit	ΔV_{avg_2} $(m/s/day)$	ΔV_{avg_1} $(m/s/day)$	$\Delta V_{radial,avg}$	$\Delta V_{tangential,avg}$	$\Delta V_{normal,avg}$
1	2.95	3.91	1.94	1.81	0.16
2	2.93	3.88	1.90	1.82	0.16
3	1.63	1.96	0.24	1.56	0.16

We also present the maximum specific force (force per kg of mass) components for each orbit:

Orbit	Max. Radial Force (μN/kg)	Max. Tangential Force (μN/kg)	Max. Normal Force (μN/kg)
1	41.2	38.7	3.4
2	41.2	36.8	3.4
3	5.3	31.8	3.4

The radial motion of the point tracked for Orbit-3 is given in Figure 13. It is computed that, 15% to 16.5% of the Sun can be observed from Orbit-3 (occultation of Sun is 84.5% to 85%). The variations of mean monthly distance of the orbit point to Earth is due to the eccentricity of the orbit of Barycenter around Sun.

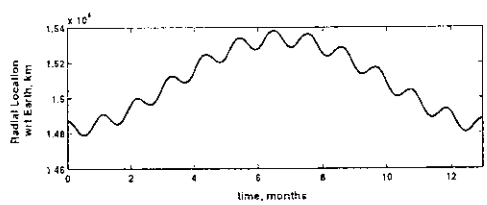

Figure 13. Motion of Orbit-3

VII. Actuation

In this section, we discuss a thruster configuration which is duplicated on both spacecraft buses. We propose a propulsion scheme, and point out some imperfections that can arise in thrusting. We use thrusters for translational control, and reaction wheels for attitude control. Since disturbance torques are very small, we can consider the reaction wheels as linear actuators for our application.

A. Thruster Configuration and Sizing

We use two sets of thrusters for translation control, ***large*** and ***small*** thrusters. Large thrusters provide feed-forward control forces as well as orbital feedback forces in radial-tangential plane. Small thrusters provide formation control forces, provide orbital feed-forward and feedback forces in normal direction (which are an order smaller than radial

and tangential components), and counteract residual forces in normal direction caused by large thruster firings (because of canted large thrusters).

We propose using electric propulsion (EP) with xenon as the fuel. Current state of the art application for EP is the ion thrusters on NASA's Deep Space-1 spacecraft.[4] The current technology can produce high specific impulses (3500 secs for DS-1 thrusters). This makes EP the most attractive choice for our application, which should last 5-10 years without re-fueling. Therefore, we need high specific impulses which will reduce the fuel requirements. The current forecasts suggest that the specific impulses (Isp) of 6000 secs for EP thrusters. This makes our mission feasible in terms of fuel requirements for a 5-10 years mission. One can observe that with a simple computation (which will also be substantiated with more complicated simulations), where we use the required ΔV values for Orbit-3. In Orbit-3, we have $\Delta V_{avg_1} = 1.96\ m/s/day$. If we assume ideal orthogonal thrusting, with $Isp = 6000$ secs, then we obtain a fuel requirement per unit mass of the payload for ten years as

$$Fuel = 10 \times 365.25 \times 24 \times 3600 \times \frac{\Delta V_{avg_1}}{24 \times 3600 \times Isp \times g} = 0.1216\ kg/kg - payload\,,$$

where g is the Earth's gravitational constant. This number gives a lower bound on the fuel requirement for a ten year mission, however, since the environmental disturbances are not substantial, we do not expect to deviate from this number significantly. Note that, this corresponds to approximately 0.94×10^{-3} kg fuel per month (28 days), per kg of payload.

The thruster configuration and sizing can be performed by using the orbital properties of the mission. Since, we follow Orbit-3 (see Section VI for a description of this orbit), we have to counteract forces which are on average significantly larger in tangential direction. Note that $\Delta V_{radial,avg} = 0.24$, $\Delta V_{tangential,avg} = 1.56$, and $\Delta V_{normal,avg} = 0.16$ (m/s/day) for this orbit, which is a measure of average accelerations to be provided for the orbit following. The peak values of thrust required in each direction per kg of payload are 5.3, 31.8 and 3.4 μN in radial, tangential, and normal directions. We propose a thruster configuration where there are four large thrusters on each face of the bus (faces which have normals to be aligned with the radial direction), canted so that their line of actions go through the nominal center of mass (CM) (which is currently assumed to be geometric center), and, if necessary, they could have gimballing capabilities to account for any minor CM motion during the mission. This canting together with thruster locations provided significantly more actuation force in tangential direction (nearly 83% of the thrust in tangential direction).

Currently, we propose to have 12 small thrusters in S/C-S, and 16 small ones in S/C-A. We present the thruster configurations in figures 14 and 15. Note that, we only presented one figure (Figure 15) for S/C-A to avoid repetition, where the only difference is having 4 additional thrusters.

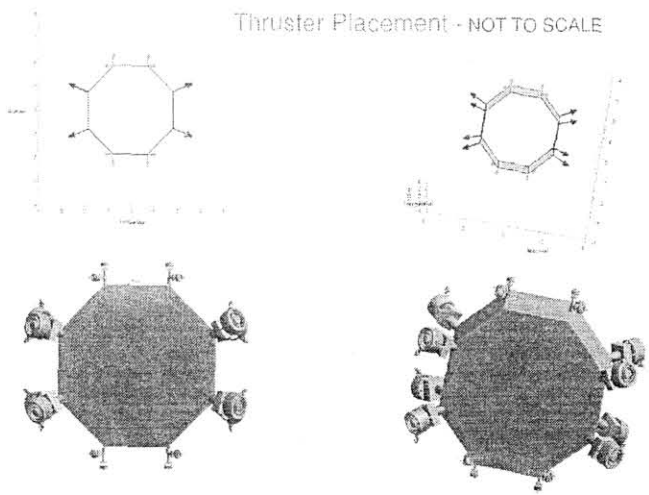

Figure 14. Thrusters

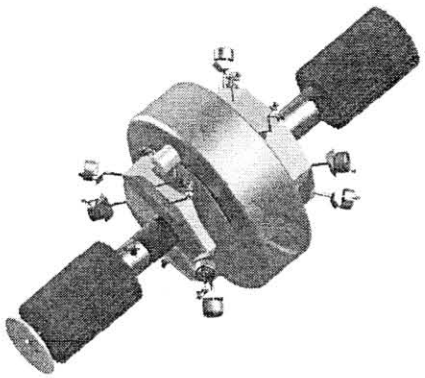

Figure 15. Thrusters on S/C-A, a predeployment configuration

While sizing these thrusters, we use the peak force corresponding to a 1200 kg spacecraft. The most critical case is when all peaks occur simultaneously, and only one thruster is assigned to counteract these orbital forces. Then the thrust needed is 39 μN per kg of payload. Accounting for feedback forces (which are assumed to be a magnitude less than feed-forward forces) and control margin, we require thrusters with 45 μ-N or larger thrust capacity per kg of payload. The small thrusters are assumed to be providing forces for formation control which counteracts differential disturbances between two spacecraft (mainly due to solar forces), so they are assumed to be providing forces of order 1-2 mN for these disturbances, as well as orbital feed-forward forces in normal direction and normal residuals from large thruster firings. Since our application has spacecraft with a mass about 1200 kg each, the normal residual forces and orbital feed-forward forces will be more critical. Therefore, we decided to use small thrusters with 5 μN peak thrust capacity per kg of payload.

Note that the number and configuration of thrusters allow us to accommodate some thruster failures. This is a desirable aspect of thruster configuration for a long duration deep space mission, where thrusters continuously fire. Further analysis and simulation results are given in.[5]

VIII. Orbit Following and Formation Control

In this section, we summarize a control strategy to keep the desired orbit and to establish fine formation control. A block diagram representation of sensing, estimation, and control is given in Figure 16, with a diagram describing subsystems in Figure 17. The spacecraft have two control modes, namely,

- Deployment mode,
- Formation mode.

In *deployment mode*, each spacecraft has its own attitude and orbit controller, and sensor. This approach provides autonomy for both spacecraft during the deployment phase. Since the formation is formed in this phase, they have to avoid collisions until the formation is established. In the *formation mode*, we have a central executive formation and orbit estimator and controller in the Science spacecraft providing the necessary formation positioning commands, which are then communicated to the aperture spacecraft controller.

The attitude and translational control actions are designed independently, by using multi input-output (MIMO) PID control strategies. In translational control, the controller bandwidth for orbit following is significantly lower than the relative position controller, because of the significant differences in accuracy between them. A Ricatti equation is solved to obtain controller gains, which also introduces robustness to the system uncertainties.[6–8] Then, a standard Kalman filter is used to estimate the states required by the controls.[9] A detailed discussion of the formation mode control is given in.[5]

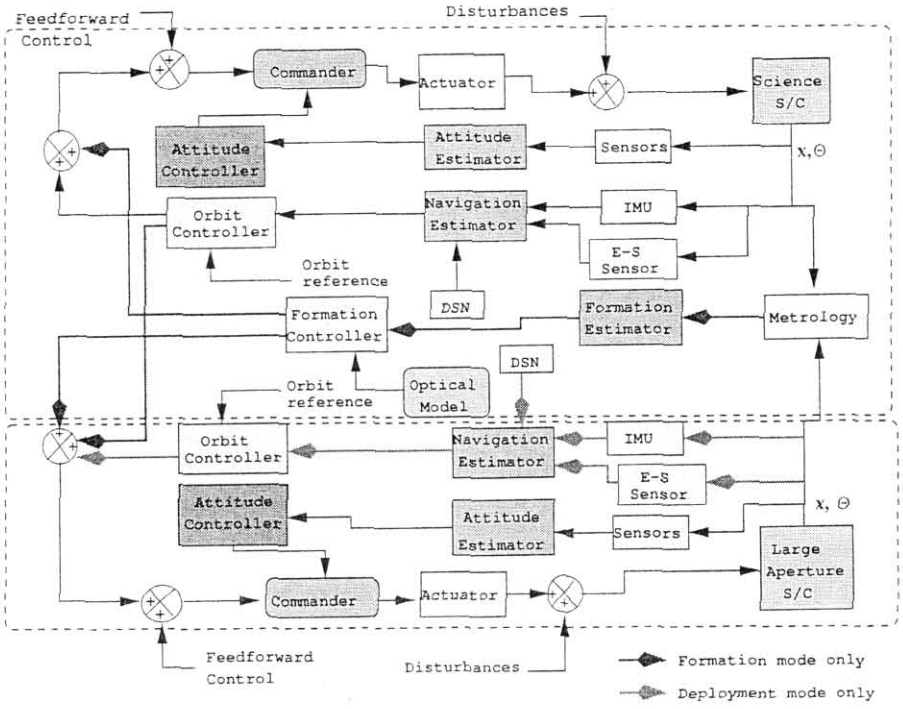

Figure 16. Estimation and Control

A. Translation Control Strategy

We have three major sets of control input,

- Feed-forward control input for mean orbit following, which is common to both spacecraft.
- Feedback control input for tracking the orbit to reject disturbances, which is common to both spacecrafts.
- Feedback control for fine formation control, which can be different for each spacecraft.

The main control objectives are:

- Keep the formation in the close neighborhood of the orbit point, i.e. the formation does not move out of a circle with center on Sun-Earth line and radius of 200 km, on the plane orthogonal to radial direction. Also, keep the radial distance from orbit point small enough so that the occultation of Sun is at reasonable (10-20 %) levels.
- Keep the formation aligned parallel to Sun-Earth line, with a distance of 125 m in between two spacecraft.

The relative dynamics of the formation is decoupled from the overall dynamics. Therefore, we design a feedback controller for the relative formation dynamics independently. The controller is a multi input-output PID controller (actually it is a multi-input single output control if we consider dynamics on each axis separately) that satisfies relative positioning requirements.

Since, we expect larger measurement errors and longer time scales for the relative position with respect to the reference orbital point, we design a feedback closed loop system with much smaller bandwidth for orbit feedback control. This implies that the response is much slower for orbit following than the formation control. We use a similar approach in designing orbital feedback control as in formation control, i.e. a MIMO PID controller is designed for orbit control.[5]

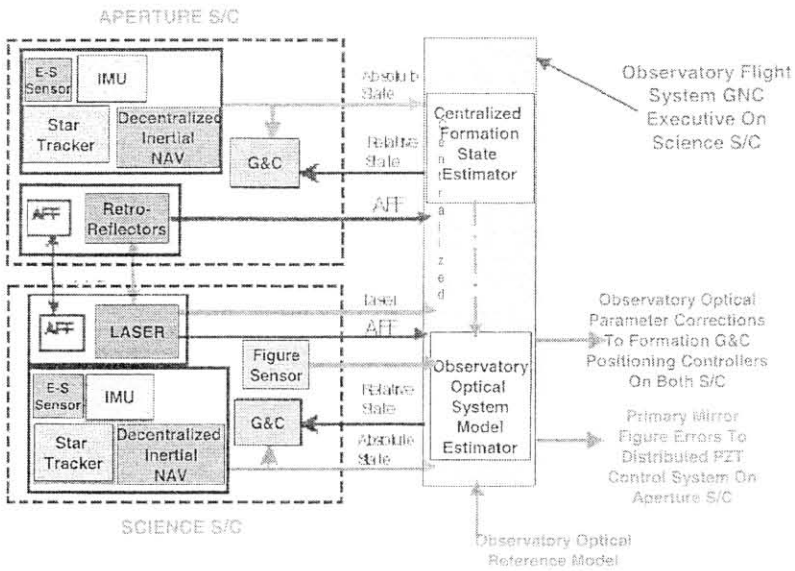

Figure 17. Estimation and Control Subsytems

IX. Primary Mirror Shape Control

In this part of the report, we discuss possible control techniques for shape control of the 25 meter primary mirror. The weight of the mirror is the most important design parameter, that motivates the development of new design concepts and technologies. Development of large, ultra-light weight space telescopes is also one of the primary technology focus areas of NASA. The proposed mirror in our application has a surface area about 450 m^2. We baseline our design in order to have a mass about 1200 kg for the Large Aperture Spacecraft, which contains the mirror, the supporting structure (inflatable torus), and the engineering bus. This implies that we must have a mirror of areal density less than 1 kg/m^2.[10,11] The current lightweight glass-based mirrors have areal densities of $15-20$ kg/m^2. Foam and SiC technologies are shown to bring this number down to $10kg/m^2$ levels, but this is still extremely heavy and unacceptable for our application. This motivates usage of ultra-light membrane type flexible mirrors. The wavefront abberations can be corrected by adaptive optics in a corrector mirror in the Science spacecraft.[12,13] However, there is no available wave front sensor technology to detect the abberations caused by the large mirror. Therefore, we propose a fine shape control of the spherical large mirror, and correction of only the spherical abberations by the corrector mirror.

There are significant technological challenges in building, deploying, and operating a lightweight membrane type mirror of such a large size:

- Producing a mirror surface of such large dimension (diameter $> 10m$), with excellent optical quality.
- Obtaining an aerial density less than 1 kg/m^2, with the supporting structure.
- Packaging, and transfer of the mirror to the orbit.
- Deploying the mirror to its science configuration without significant deformations.
- Sensing the shape of the mirror once it is deployed: Designing the sensors, and estimation algorithms to achieve fine sensing.
- Fine control of the mirror shape: Structural design of the mirror, actuator design, development of appropriate control algorithms.

Currently, there is not a such large size membrane type mirror operating in space. Therefore, all of the issues listed above, have to be carefully studied. For comparison, the current light weight large area, James Webb telescope, has a 6 meter diameter, and an aerial density of about 15 kg/m^2, with a segmented rigid structure. A wavefront sensing and

control approach is used to control the shape of the deformable glass mirror, where actuator commands are generated separately for each segment.[14] In our application, we have a much larger size monolithic mirror, which is made up of a deformable membrane, with a significantly less aerial density. And current wave front sensing techniques only consider abberations from a point source of light. However, abberations caused by the primary mirror, which does not image a point source of light, must be sensed in our application. Therefore, current wavefront sensing and control techniques for adaptive optics can not readily be applied. Consequently, we propose another approach where we control the shape of the large mirror so that it has a perfectly spherical shape (as much as possible), so that the reflected light only have spherical abberations, which are then corrected by optics in the Science Telescope.

Our objective is to identify a possible architecture for the design of the large mirror, to identify existing technological capabilities as well as future technologies to be developed, and assess the feasibility of such structure in general. In this perspective, we specifically address some of the issues listed above, and propose possible solutions to the technical challenges involved.

A. A Shape Control Strategy for the Membrane Mirror

We consider a combined approach of depositing an optical quality reflecting surface onto a Nitinol shape memory alloy (SMA) 5 micron membrane that has been precondition to deploy to nominally spherical shape. Two layers of 10 micron orthogonally polarized piezoelectric membranes are bounded behind the SMA. The desired deformations to control the spherical shape are obtained by applying voltage distributions through a unique pattern of sparsely deposited electrodes that locally contract or expand the piezo-material to cause bimorph actuation (biaxial bending) for precision shape control. We carry out a fine wavefront control of the large membrane as a "Schmidt" mirror, and leave only residual spherical abberations corrected by a small adaptive Schmidt corrector optics in the receiver telescope on the secondary spacecraft.

The mirror, in our application, is supported by an inflatable torus in the inner and outer rim. The mirror geometry and the shape control concept are shown in figures 18, 19, and 20. The connection of the inner and outer torus to the mirror is accomplished by an *interface* region which is composed of PVDF strips connecting the mirror to the torus. PVDF is used because of its low modulus of elasticity. Their back surface can have MEMS inchworm actuators[10] (which are capable of large strokes of about 250 microns), and they are connected to torus via a large stroke piezo actuator. Therefore, the PVDF connector strips can be controlled such that the internal forces and moments at the joints with the mirror are minimized. By minimizing these reaction forces and moments, a soft connection between the mirror and the torus is established that prevents the transfer of any external forces from the torus to the mirror. There are strain gages allocated on the connector strips, which provide the necessary data in order to compute the feedback action to minimize the reaction forces.

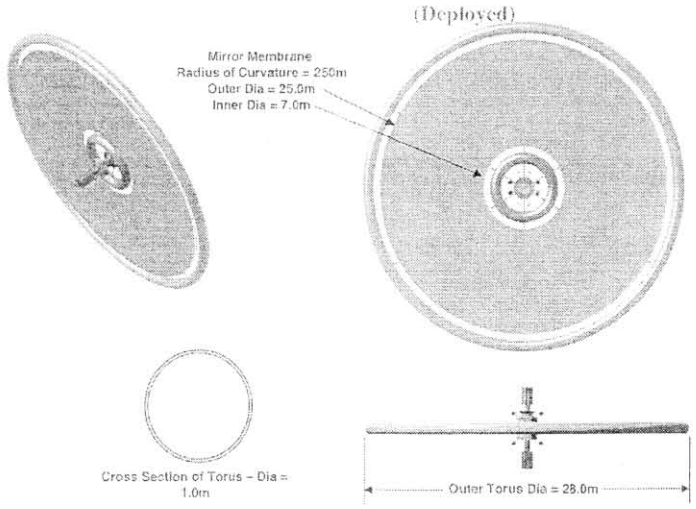

Figure 18. The Large Mirror

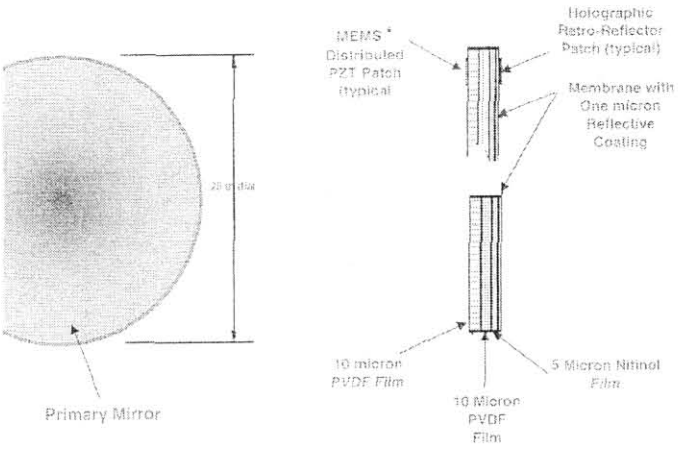

Figure 19. Shape Control

The control forces and torques for shape control[5] are generated by applying voltage to expand or contract bonded piezoelectric actuators. Some choices for piezoelectric materials for our application are PVDF (polyvinylidene fluoride), PZT, Polyurethane, which have different mass, strength, and thermal properties. The following table summarizes the mechanical properties of the materials (SMA and piezo materials) considered for our design [c]:

Material	PZT-5A	PVDF	Nitinol
Type	Piezo-Ceramic	Piezo-film	SMA
Poisson's Ratio	0.31	0.35	0.33
Young's Modulus (GPa)	62	1.2	35(mar.), 83 (aus.)
CTE (ppm/°C)	3.5	42	7 (mar.), 11 (aus.)
Density (g/cm^3)	7.8	1.77	6.5

aus. : austenite
CTE : Coefficient of Linear Thermal Expansion Especially PVDF is an attractive piezo-material for lightweight deformable mirror applications, because it has small density, it is flexible, and it can be cut into any shape. Also, note that PVDF has a rather small modulus of elasticity when compared with PZT or Nitinol, which makes it a good choice as a connector in order to establish a very soft joint between the torus and the mirror. PZT has more comparable stiffness and thermal properties with SMA than PVDF, so usage of PZT as the material for piezo-actuators is also considered. But, manufacturing of such thin piezo-ceramic films is more difficult than producing PVDF films, and it is a currently ongoing research and development activity. On the other hand, if PVDF is used, it must be significantly thicker than the SMA layer, in order to be able to provide sufficient actuation authority.

The MEMS inchworm actuators are shown to be highly effective for adaptive optics with small diameter mirrors. Therefore, usage of those actuator patches for very fine, high order wave front correction in the Science spacecraft (where the optical system is located) can be considered. This is an adaptive optics solution, where we compensate for optical effects introduced by the medium between the object and its image. Here, the back of the *corrector mirror* (optical element that can change the wavefront of a beam) can be covered with a high density of such actuators. A good model of the dynamics of the mirror together with very fine actuation authority can lead to a very accurate wave front correction. Since, the corrector mirror is rather small in diameter, such fine control approach is feasible. However, any adaptive optics in the corrector mirror is out of the scope of this document. There are technical difficulties in wave front sensing of the waves reflected from the large mirror, and it should be further studied to make adaptive optics for corrector mirror a feasible option as an improvement on our current design concept. Our current baseline design

[c]Material properties are provided by[15,16]

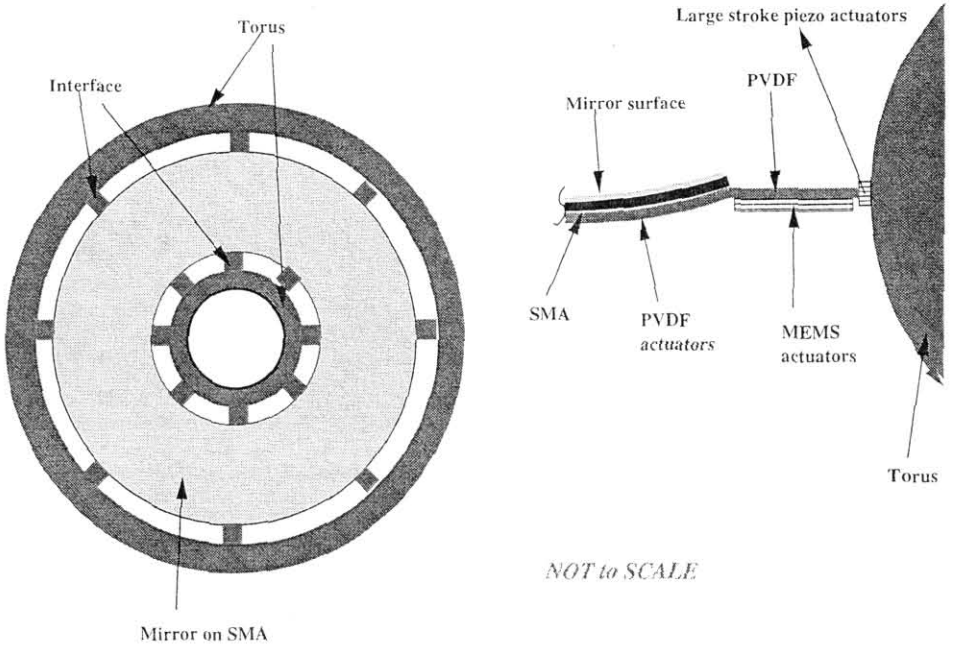

Figure 20. Shape Control

concept considers a corrector mirror which corrects only for *spherical wavefront abberations*, which are caused by the ideal spherical large mirror. Therefore, we propose to establish fine shape control of the large mirror in order to maintain as ideal spherical shape as possible.

Based on the brief discussion above, our assessment is that, fine control of the nominal shape of the large mirror via a SMA structure together with piezo actuation can achieve a desired optical performance. The following is a brief list of potential challenges in our baseline design, and possible improvements and alternatives that needs further research:

- Manufacturing the optical quality membrane material desired for the large refelector surface.
- Developing a sensor technology, in terms of hardware and estimation software, to precisely measure the mirror surface, and estimate the deformations.
- Analyzing and mitigating the shape errors caused by differences in thermal properties, i.e. different coefficient of thermal expansions for bonded surfaces.
- Development of models describing the dynamics of the membrane together with the actuation.[17]
- Development of efficient control algorithms, which can establish shape control to desired accuracies, with realizable actuation.[18] Since very accurate control of a nominal shape should be accomplished by a feasible approach, we do want to develop techniques that will not require enormous number of actuation points or unrealistic computational overhead, while being smart enough to satisfy design requirements. Therefore, research on designing an optimal sparse distribution of electrodes for piezo-actuation to obtain the desired control authority is essential.
- Development of a wavefront sensor technology for the adaptive optics in the corrector mirror. This will significantly enhance the feasibility of our baseline approach, which relies on very fine control of the large mirror, by relaxing the requirements on the accuracy of the shape control. Then, the large mirror shape control objective will be the correction of wavefront errors which are beyond the dynamic range of the adaptive small corrector mirror.

The modelling of the dynamics and control of the large mirror has two major steps, (see[12,17,19–21] for modelling of membranes, and piezoelectric actuators):

- Modelling the response of the piezoelectric material to the electrical excitation.[22,23]

- Modelling of nonlinear dynamics of thin shell mirror (mirror at its nominal spherical shape) together with the dynamics of piezoelectric material.

We propose a quasi-static modal control approach for the large mirror shape control.[5] In this approach, the shape of the mirror is given in terms of orthonormal polynomials defined on a unit disk, which are known as Zernike polynomials.[13] Then, an algorithm that computes the required actuation will adjust the coefficients in these series in order to establish the desired spherical mirror shape.

Acknowledgments

This research was performed at the Jet Propulsion Laboratory, California Institute of Technology, under the contract with National Aeronautics and Space Administration. We wish to gratefully acknowledge the membrane modeling advice of Drs. S. S. Lih, E. H. Yang, and M. B. Quadrelli of JPL, and J. Pellicciotti and C. Strickland of LaRC for structures and material technology advice. We also gratefully acknowledge J. Antol of NASA LaRC for his RASC program support, R. Manvi and C. Weisbin of JPL for their task coordination and integration efforts.

Finally, we wish to gratefully acknowledge teh many other subsystem specialists at NASA GSFC and GRC who contributed to the overall concept definition study of the Earth Atmosphere Observatory at L2.

References

[1]Lay, O. P., Dubovitsky, S., Peters, R. D., Burger, J. P., Ahn, S.-W., Steiner, W. H., Fetterman, H. R., and Chang, Y., "MSTAR: A submicrometer absolute metrology system," *Optics Letters*, Vol. 28, No. 11, 2003.

[2]Marr, G. and McGuire, M. L., "Internal Communication," *NASA Goddard Space Flight Center*, 2003.

[3]Roy, A. E., *Orbital Motion, 3rd Edition*, University of Physics Publishing, 1988.

[4]Brophy, J. R., Kakuda, R. Y., Polk, J., Anderson, J., Marcucci, M., Brinza, D., Henry, M., Fujii, K., Mantha, K., Stocky, J., Sovey, J., Peterson, M., Rawley, V., Hamley, J., Bond, T., Christensen, J., Cardwell, H., Benson, G., Gallagher, J., Matranga, M., and Bushway, D., *Ion Propulsion System (NSTAR) DS-1 Technology Validation Report, NASA Jet Propulsion Laboratory*.

[5]Açıkmeşe, A. B., Mettler, E., Breckenridge, W. G., Macenka, S. A., and Tubbs, E. F., "L2 Earth Atmosphere Observatory: Formation Guidance, Metrology, and Control Synthesis," *AIAA/AAS, Astrodynamics Specialists Conference, Providence R.I.*, August, 2004.

[6]Açıkmeşe, A. B. and Corless, M., "Robust Constant Output Tracking for Uncertain/Nonlinear Systems with PI Controllers," *American Control Conference*, 2001.

[7]Açıkmeşe, A. B. and Corless, M., "Robust Output Tracking for Uncertain/Nonlinear Systems Subject To Almost Constant Disturbances," *Automatica*, Vol. 38, No. 11, 2002.

[8]Corless, M. and Frazho, A. E., *Linear Systems and Control: An Operator Perspective*, Marcel Dekker, 2003.

[9]Gelb, A., *Applied Optimal Estimation*, The M.I.T. Press, 1974.

[10]Gullapalli, S. N., Flood, R., Yang, E. H., and Lih, S. S., "New Technologies for the Actuation and Control of Large Aperture Lightweight Optical Quality Mirrors," *Proceedings of IEEE Aerospace Conference*, Vol. 4, 2003.

[11]Yang, E. H., Schheglov, K., and Trolier-McKinstry, S., "Concept, Modelling and Fabrication for Large-Stroke Piezoelectric Unimorph Deformable Mirrors," *JPL Internal Document*.

[12]Ellis, E. M., *Low-Cost Bimorph Mirrors in Adaptive Optics*, Thesis, Imperial College of Science, Technology, and Medicine, University of London, 1999.

[13]Tyson, R., *Principles of Adaptive Optics*, Academic Press, 1997.

[14]Redding, D., Basinger, S., Lowman, A. E., Shi, F., Bely, P., Burg, R., and Moiser, G., "Wave Front Control for the Next Generation Space Telescope," *www.ngst.nasa.gov*.

[15]Pellicciotti, J., "Internal Communication," *NASA Goddard Space Flight Center*, 2003.

[16]Strickland, C., "Internal Communication," *NASA Langley Research Center*, 2003.

[17]Quadrelli, M. and Sirlin, S., "Modeling and control of membranes for gossamer spacecraft. Part 1: Theory," *42nd AIAA/ASME/ASCE/AHS/ASC Structures, Structural Dynamics, and Materials Conference*, 2001.

[18]Zhu, L., Sun, P., Bartsch, D. U., Freeman, W. R., and Fainman, Y., "Adaptive Control of a Micromachined Continuous-Membrane Deformable Mirror for Abberation Compensation," *Applied Optics*, Vol. 38, No. 1.

[19]Hickey, G. S., Lih, S. S., and Barbee, T., "Development of Nanolaminate Thin Shell Mirror," *JPL Internal Communication*, 2003.

[20]Lih, S. S., Hickey, G. S., Ding, J. H., and Tzou, S. H., "Micro-Control Actions of Segmented Actuators on Shallow Paraboloidal Shell Reflectors," *ASME International Adaptive Structures and Materials Systems Symposium*, 2002.

[21]Ellis, E. M., *IEEE Standard on Piezoelectricity, ANSI/IEEE Standard 176-1987*, IEEE, 1987.

[22]Tzou, H. and Howard, R. V., "A Piezothermoelastic Thin Shell Theory Applied to Active Structures," *ASME Transactions, Journal of Vibration and Acoustics*, Vol. 116, 1994, pp. 295–302.

[23]Tzou, H. and Ye, R., "Piezothermoelasticity and Precision Control of Piezoelectric Systems: Theory and Finite Element Analysis," *ASME Transactions, Journal of Vibration and Acoustics*, Vol. 116, 1994, pp. 489–495.